Available online at www.sciencedirect.com
SCIENCE DIRECT
Talanta 68 (2006) 1692–1699
Talanta
www.elsevier.com/locate/talanta

Development and optimisation of a portable micro-XRF method for in situ multi-element analysis of ancient ceramics

D.N. Papadopoulou [a], G.A. Zachariadis [a], A.N. Anthemidis [a], N.C. Tsirliganis [b], J.A. Stratis [a,*]

[a] *Laboratory of Analytical Chemistry, Faculty of Chemistry, Aristotle University, GR-54124 Thessaloniki, Greece*
[b] *Archaeometry Laboratory, Cultural and Educational Technology Institute, Tsimiski 58, GR-67100 Xanthi, Greece*

Received 18 April 2005; received in revised form 1 August 2005; accepted 10 August 2005
Available online 19 September 2005

Abstract

Non-destructive analysis of cultural objects by micro-XRF spectrometry is an advantageous multi-element technique that has rapidly developed during the past few years. Portable instruments contribute significantly to the in situ analysis of valuable cultural objects, which cannot be transported to the laboratory. Ancient ceramics are the most common archaeological findings and they carry a significant historical content. Their analysis often presents certain particularities due to surface irregularities and heterogeneity problems. In the present work, the analytical characteristics (beam spot size, geometry effect and detection limits) of a compact and portable micro-XRF instrument with a monocapillary lens are presented in details. The standard reference materials SARM 69, SRM 620, NCS DC 73332 and the reference materials AWI-1 and PRI-1 were analysed for the determination of the detection limits (DL's) and the evaluation of the accuracy of the micro-XRF. Emphasis is given on the critical parameters, which should be monitored during measurements and influence the final results in the analysis of ancient ceramics. A quantitative analysis of ancient ceramic samples from Abdera (North Greece) is also presented.

Keywords: Micro-XRF; In situ analysis; Ancient ceramics; Portable instruments; Non-destructive analysis

1. Introduction

The potential of using X-rays in the qualitative and quantitative analysis of several different samples was appreciated soon after their discovery. Since then, a large variety of instrumental techniques, employing the use of X-rays, have been developed and can be successfully applied for the study and conservation of cultural objects [1,2]. Among these, X-ray fluorescence spectroscopy is the most widely used technique due to a number of favorable analytical characteristics, such as multi-element analysis, non-destructive analysis, high sensitivity and applicability to a wide range of samples (solids, liquids and gases) [3–5]. These features have made XRF a very popular analytical technique in several archaeometric studies [1,5–8].

Micro-X-ray fluorescence spectroscopy, the microscopic equivalent of bulk XRF, is one of the most modern and promising branches of XRF, which permits the precise, accurate, non-destructive and localized analysis of small objects or of details on larger ones [9,10]. The implementation of capillary optics for focusing X-ray beams, which was introduced in the mid-80s, has contributed significantly to the development of several new scientific instruments [11–14]. The ability to obtain point spectra and elemental maps have lead to numerous applications of micro-XRF on the analysis of different types of materials, including metallic objects, industrial materials, forensic samples, gold artifacts, bronze statuettes, paint layers, etc. [15–19]. More recently, the need to perform in situ analysis of cultural objects, which cannot be transported to the laboratory, has lead to the development of portable micro-XRF spectrometers [20–22]. This was facilitated by the development of small-sized Peltier-cooled energy dispersive detectors and X-ray optics [20,21].

Information on the applicability of the portable micro-XRF instruments and thorough examination of their analytical characteristics is useful for their evaluation but is rarely found in the literature. Such integrated information concerning the analytical characteristics of a portable micro-XRF with monocapillary

* Corresponding author. Tel.: +30 2310997843; fax: +30 2310997719.
E-mail address: jstratis@chem.auth.gr (J.A. Stratis).

0039-9140/$ – see front matter © 2005 Elsevier B.V. All rights reserved.
doi:10.1016/j.talanta.2005.08.051

optics and its application for the in situ analysis of ancient ceramics is presented in this paper with emphasis on the effect of certain critical parameters on the analysis.

Quantitative measurements were performed on ceramic and glass standard reference materials. Similar measurements were performed for the quantitative analysis of ancient ceramics, which represent a large class of cultural objects with important historical content.

2. Experimental

2.1. Instrumentation

The micro-XRF spectrometer (SPECTRO, COPRA model) used in this work includes a side-window X-ray tube with Mo anode (Oxford Instruments, Series 5011 XTF), a straight monocapillary lens and a solid state Si(Li) Peltier-cooled detector (8 μm Be window, 3.5 mm^2 active area, 300 μm nominal thickness). The maximum tube voltage is 50 kV and its maximum current 1 mA. The nominal energy resolution of the detector for Mn K_a is 149 eV at a count rate of 1 kcps, while the measured resolution is 151, 154, 190, 151 and 171 eV for the K K_a, Ca K_a, Ca K_b, Fe K_a and Fe K_b lines, respectively, at a total count rate of 1.3 kcps.

A long-distance optical microscope located on the detector and X-ray tube plane is used in order to select the points of interest over the surface of the sample (Fig. 1). The samples which are placed on a rotating holder mounted on a motorized *XYZ* stage, consisting of three linear stages by NewPort (PRL-12) featuring 0.1 mm step size, travel distance of 5 cm in the *X*–*Y*-direction and 2.5 cm in the *Z*-direction are moved so that the points of interest lie in the focal plane of the long-distance optical microscope. At this position, the angle of incidence of the primary beam is 48°, while the angle between the sample and the detector is 42°. All measurements are performed in air and no filters were used. The micro-XRF experimental set-up and the respective geometry are shown in Fig. 1. The angle between the primary beam and the detector axis with respect to the surface of the sample can be changed by rotation of the sample. The relative angle between the X-ray tube and the detector is fixed by the manufacturer at 90° and remained unchanged during the measurements. All measurements are performed in air and no filters were used.

All micro-XRF measurements were performed in a point scan mode. X-ray spectra were deconvoluted by a dedicated software package (WinAxil v 4.0.1). In particular, spectral data are processed by the method of non-linear least squares fitting, where the optimum values of χ^2 (the weighted sum of squares of the differences between a chosen model and the measured spectrum) are found iteratively (Marquardt algorithm).

2.2. Samples and standard reference materials

The investigated ceramic sherds were excavated in the ancient cemetery of Abdera (North Greece) and they date back to the 5th and 7th century B.C. Quantitative analysis was performed for the samples coded A45, A46, A47, A48, A51, A53, A56, A57, A58, A78, A118 and A119. According to the archaeological information, samples A57, A58, A118 and A119 are suspected to be imported products, while the remaining samples are regarded as local products. All samples were cleaned by distilled water and oven-dried at 105° C until constant weight before analysis.

The effect of the incident angle of the primary X-ray beam on the elemental peak area was investigated for three ancient ceramic sherds each representative of a different grain size distribution (fine, medium and coarse texture). The characterization fine, medium and coarse was assigned after the investigation of the three sherds under a polarizing microscope without any further quantitative justification, since this exceeded of the scope of the present work.

Three standard reference materials and two reference materials were used. The standard reference material SARM 69 is prepared and distributed by MINTEK South Africa and the Department of Geology, University of Free State, the SRM 620 (soda lime flat glass) is prepared by the National Institute of Standards and Testing and the SRM NCS DC 73332 is prepared by China's National Analysis Center for Iron and Steel. The reference materials AWI-1 and PRI both from Group of Instrumental Geochemistry, Fonds National de la Recherche Scientifique/Nationaal Fonds Voor Wetenschappelijk, FNRS-NFWO were also used. All standards (except for SRM 620 which is in the form of a wafer) were analysed in the form of pressed

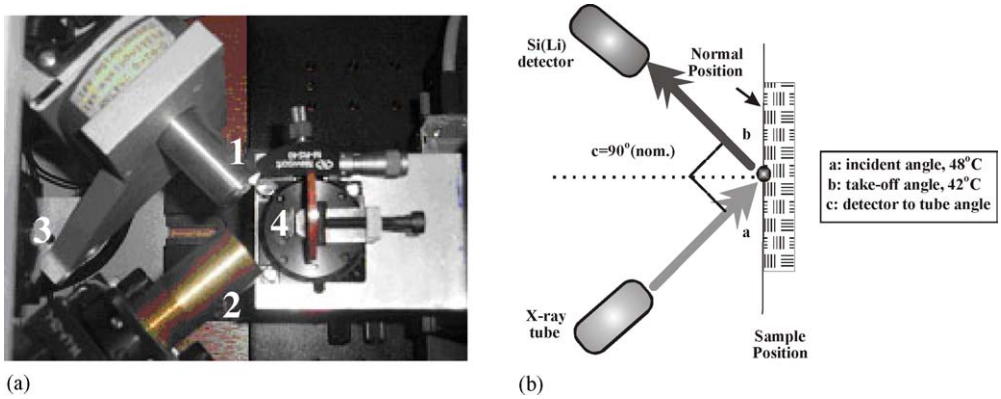

(a) (b)

Fig. 1. (a) Micro-XRF spectrometer: (1) X-ray tube and monocapillary system; (2) Si(Li) detector; (3) optical microscope; (4) sample holder and sample. (b) Schematic diagram of the experimental micro-XRF geometry.

pellets prepared by mixing with a cellulose binder and pressing in a hydraulic press (11 t). The standard glass SRM 620 was chosen in order to apply the micro-XRF method to a second silicate material that presents archaeological interest. It was outside the scope of the present work to prepare fused beads, since our present interest lies in the non-destructive analysis of ancient ceramics.

The two standard reference materials SARM 69 and SRM 620 were used for the determination of the detection limits (DL's). The accuracy of the micro-XRF was evaluated by analyzing all five standard reference materials. All the ancient ceramic sherds and the pressed pellets are regarded as thick samples in the micro-XRF analysis.

3. Results and discussion

3.1. Spot-size measurements

In order to characterize the primary X-ray beam size, a 50 μm Ni wire was scanned perpendicularly to the beam in steps of 0.05 and 0.1 mm (with the wire positioned on the focal plane). The net peak area of the Ni K_a line at 7.477 keV was recorded as a function of the relative position (distance) of the wire on the focal plane with respect to the X-ray beam position and the full width at half-maximum (FWHM) of this distribution was calculated (Fig. 2).

The procedure was repeated for different positions of the wire relative to the focal plane (for an overall distance of 2 mm in steps of 0.05 and 0.01 mm, from +1 to −1 mm, where $z = 0$ represents the position at the focal plane) and the values of the FWHM were plotted against the relative distance from the focal plane (Fig. 3).

The value of the FWHM decreases as the sample approaches the monocapillary end (positive distance values in Fig. 3), verifying that the spot-size of the X-ray beam, which is produced by the monocapillary is dependent on the position of the sample relative to the focal plane. This effect is also depicted in Fig. 4 for two marginal distance values of the Ni wire relative to the focal plane.

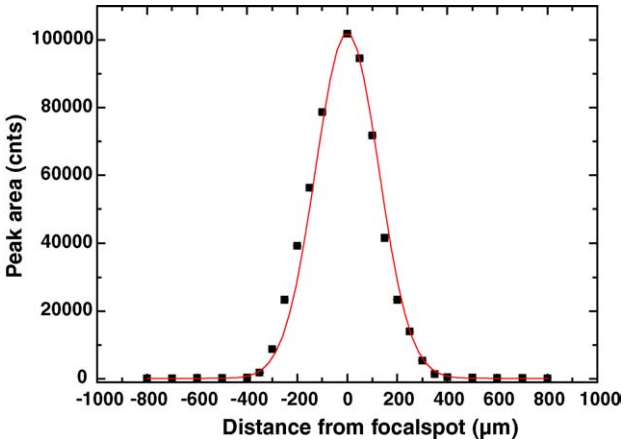

Fig. 2. Determination of FWHM of the incident beam using a 50 μm Ni wire.

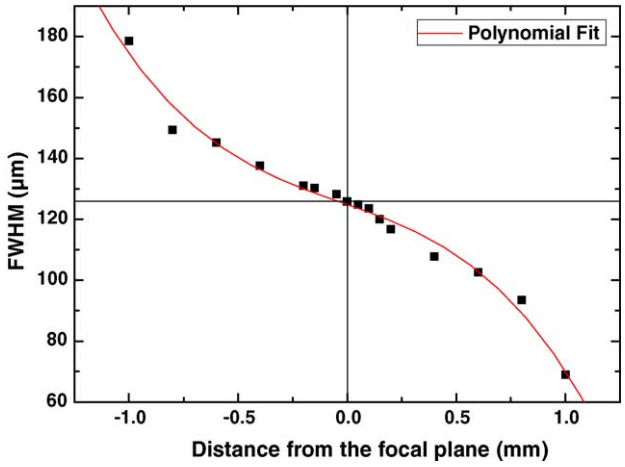

Fig. 3. Dependence of the FWHM on the relative distance from the focal plane.

A beam diameter of 126 μm was determined on the focal plane. Although smaller spot-sizes can be achieved in the current portable micro-XRF spectrometer by moving the sample closer to the monocapillary end, the sample should be kept in the focal place ($z = 0$), so that the primary beam and the detector are kept in a 90° geometry, where the scatter effects are minimized [23].

3.2. Geometry influence

The standard geometry of the micro-XRF spectrometer according to the manufacture when the sample is positioned at the focal plane is 48°/42° (angle between primary beam and the sample and angle between detector and the sample, respectively). In order to examine the influence of the angle of incidence of the primary beam on the sample, a focal spot was chosen on the rotation axis of the sample and the X-ray spectra were recorded as a function of the angle of incidence by rotating the holder in steps of 4°. Overall, the value of the incidence angle of the X-ray micro-beam ranged between 12° and 88°.

In particular, the effect of the incident angle of the primary X-ray beam on the peak area was investigated for the six most

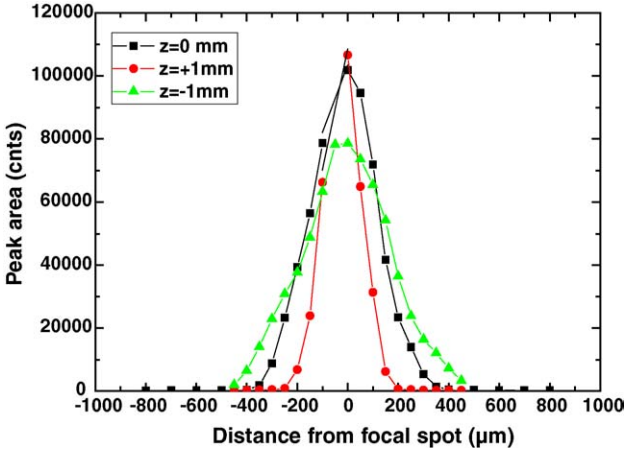

Fig. 4. Determination of the FWHM for three different distances from the focal plane (where $z = 0$ mm on the focal plane, $z = +1$ mm in front of the focal plane towards the capillary and $z = -1$ mm behind the focal plane).

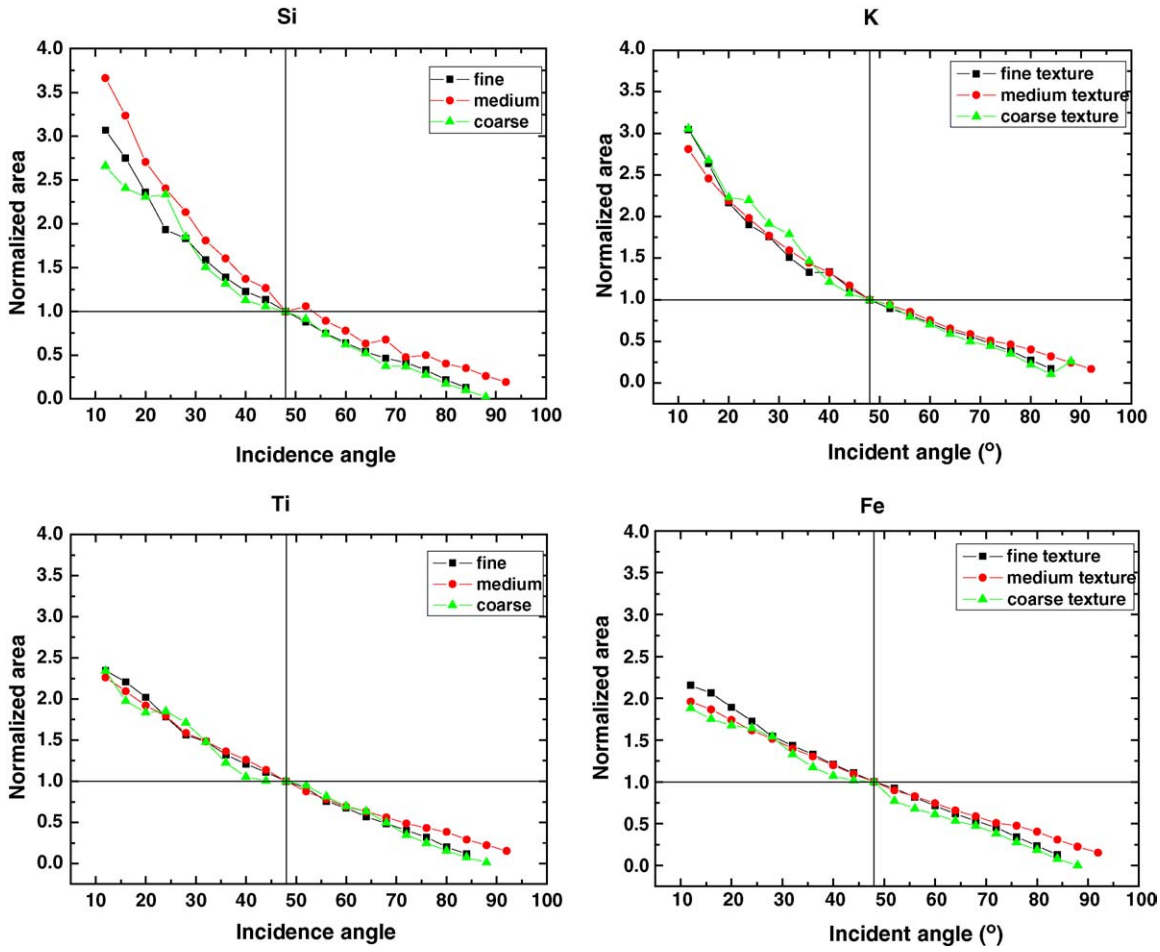

Fig. 5. Normalized peak area's dependence on the incidence angle of the primary X-ray micro-beam.

prominent characteristic lines determined in the ceramic samples (Si K_a, K K_a, Ca K_a, Ti K_a, Mn K_a and Fe K_a). As a general observation, the peak areas of all characteristic lines are decreased with increasing values of the incidence angle (Fig. 5). For the ceramic sample of fine texture a relative smooth reduction trend is observed. A similar behavior was observed in the case of the ceramic sample of medium texture with only a couple of noted irregularities (namely for Si and Mn). On the other hand, in the case of the coarse ceramic sample an erratic behavior was observed for many elements (e.g. Ca, Mn and Fe) indicating a dependence of the micro-XRF analysis on the grain size distribution of the analysed sample. It is also noted that the shape of the curve for the fine texture ceramic is hyperbolic for K and it becomes almost linear in the case of Fe. The different reduction pattern of the peak area versus the angle of incidence is attributed to the energy value of the characteristic lines.

For an angle difference of ±4° relative to the normal measurement geometry, the peak area reduction can range from 8 to 14% for a fine texture sample and from 6 to 26% for a medium texture sample, respectively.

The reduction of the element peak areas with increasing values of the incidence angle is related to the cross section of the beam, which is also reduced as the incident angle of the X-ray beam increases. This phenomenon is optically demonstrated by the trace of the X-ray beam as it was recorded on a fluorescent paper for different values of the incident angle (Fig. 6).

The above indicate that the angle of incidence is a critical parameter. Small variations in the value of the angle of incidence can influence the peak area values and consequently the quantitative results. Special care should be taken so that the incidence angle of the primary X-ray beam is reproducible between repeated measurements. The influence of this parameter

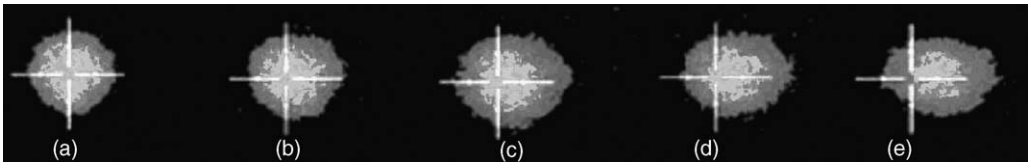

Fig. 6. X-ray beam trace for different values of the incident angle of the primary X-ray beam: (a) 62°; (b) 54°; (c) 48°; (d) 42°; (e) 34°.

Table 1
Detection limits (DL) obtained for standard reference materials SARM 69 and SRM 620

Element or element oxide	DL (mg kg^{-1})	
	SARM 69	SRM 620
Si	0.260[a]	0.170[a]
K	62	57
Ca	48	39
Ti	26	7.9
Cr	12	
Mn	19	
Fe	15	8.4
Cu	7	
Zn	11	

[a] % (w/w).

should be considered when measurements are performed on ancient ceramic sherds that exhibit surface irregularities. Sample preparation considerations that arise in this case regarding solid samples are the need of surface flattening or the preparation of pressed pellets.

3.3. Detection limits

The detection limits were determined as 3 s values for a ceramic (SARM 69) and for a glass standard reference material (SRM 620). The X-ray source tube operational parameters during these measurements were 40 kV, 0.9 mA and the spectrum acquisition real time was 1000 s. Characteristic X-ray spectra of the standards analysed are presented in Fig. 7. It should be noted that laboratory built micro-XRF instruments are most often used for the analysis of low to medium atomic number elements, while heavier elements that are present in low concentrations are not often detected. The low detection efficiency of elements with $z < 14$, is resulted mainly from the absorption of their energy in the air path between the sample surface and the detector. Therefore, the available micro-XRF system cannot be used for the determination of lightweight elements like Na and Al. Silicon is detected and quantified by the present instrument, since it is a main constituent element of the calibration standards used.

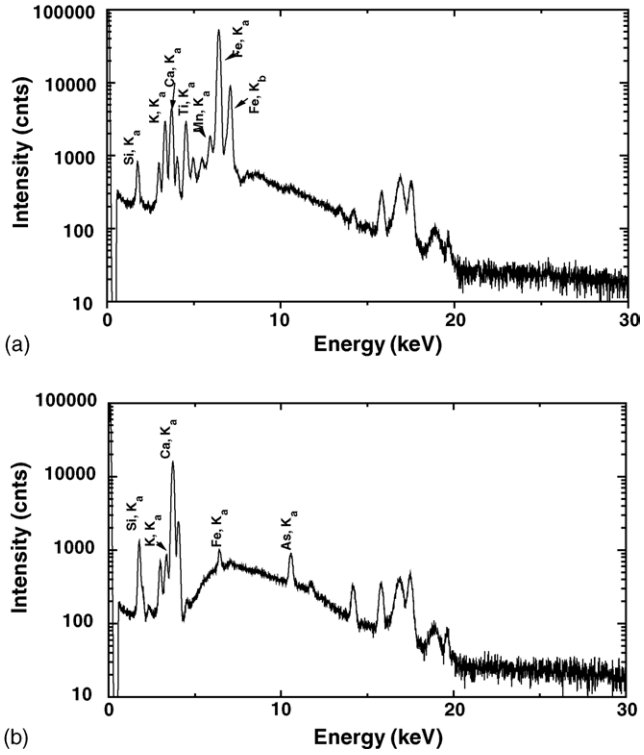

Fig. 7. Micro-XRF spectra for: (a) SARM 69 and (b) SRM 620.

Table 2
Quantitative analysis by micro-XRF for the reference materials SARM 69, NCS DC 73332, SRM 620, AW-I and PR-I (concentrations in % (m/m) ± S.D.)

	SiO_2	K_2O	CaO	TiO_2	MnO	Fe_2O_3
SARM 69						
Micro-XRF	69.1 ± 0.8	2.20 ± 0.01	2.33 ± 0.03	0.889 ± 0.039	0.149 ± 0.001	8.36 ± 0.06
Certified[a]	66.6 ± 0.5	1.96 ± 0.04	2.37 ± 0.04	0.777 ± 0.008	0.129 ± 0.002	7.18 ± 0.07
SRM 620						
Micro-XRF	78.30 ± 0.36	0.35 ± 0.00	5.96 ± 0.09			
Certified[b,c]	72.08 ± 0.08	0.41 ± 0.03	7.11 ± 0.05			
NCS DC 73332						
Micro-XRF	67.20 ± 0.90	1.05 ± 0.01	1.11 ± 0.04	0.120 ± 0.005	0.088 ± 0.002	3.89 ± 0.02
Certified[b,d]	(72)	(1.35)	(1.80)	0.100 ± 0.003	0.100 ± 0.002	(4.0)
AW-I						
Micro-XRF	59.45 ± 0.90	3.06 ± 0.04	0.73 ± 0.07	0.95 ± 0.03	0.16 ± 0.00	7.93 ± 0.06
Recommended[b]	60.46 ± 0.55	3.06 ± 0.09	0.69 ± 0.07	0.92 ± 0.05	0.14 ± 0.01	7.21 ± 0.17
PR-I						
Micro-XRF	64.50 ± 0.98	3.40 ± 0.04	2.70 ± 0.07	0.67 ± 0.02	0.06 ± 0.00	3.32 ± 0.02
Recommended[b]	68.60 ± 0.35	3.79 ± 0.21	2.49 ± 0.16	0.71 ± 0.03	0.04 ± 0.01	3.32 ± 0.13

[a] The certified values are followed by their standard uncertainty.
[b] The certified and reference values are followed by their uncertainty as stated in the relevant certificates.
[c] SRM 620 is not certified for MnO oxide concentration. The certified concentrations for TiO_2 and Fe_2O_3 oxide are low (0.018 and 0.043%, respectively) and were not quantified by the current micro-XRF measurement conditions.
[d] Values in parentheses are recommended values.

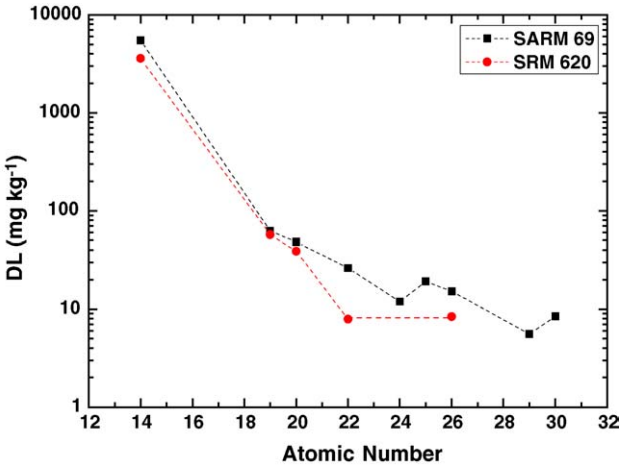

Fig. 8. Detection limits for SARM 69 and SRM 620.

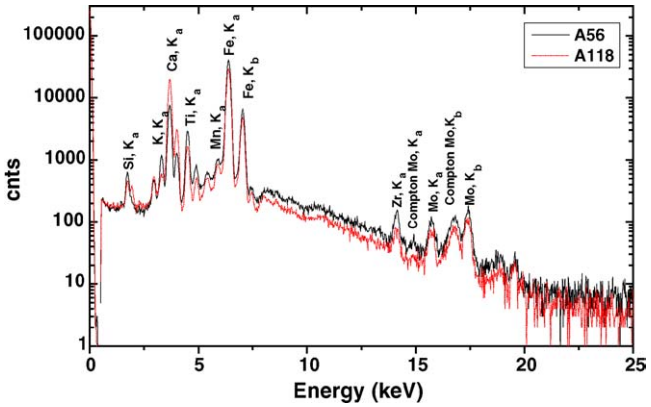

Fig. 10. Micro-XRF spectra of two ancient ceramic sherds.

The DL's determined are in the order of 7–30 mg kg^{-1} for elements with atomic number 19–30 (Table 1, Fig. 8). For similar acquisition times, systems with a monocapillary have lower intensity gains in comparison with systems that employ a polycapillary, resulting thus in higher DL's in the case of monocapillary optics [12,14].

3.4. Quantitative analysis

Several reference materials were quantitatively analysed by the portable micro-XRF spectrometer in the present and an earlier work [24]. The A number of points was chosen on each pellet and the concentrations of each element represents the mean values estimated for each of these points. The conversion of the fluorescence intensities to elemental concentrations was performed automatically by a fundamental parameters correction procedure presented in detail in Ref. [24]. The used software allows the calibration of the system by the fundamental parameters method with a single standard and the quantitative analysis of samples in a "compare" mode, where it is assumed that the calibration standard and samples have similar matrix compositions. The software used calculates the calibration curves internally.

The results of the quantitative analysis are presented in Table 2. The standard reference material SARM 69 that was used as a calibration standard was also measured as a sample. In general, there is a good agreement between the certified and the experimental values. The relative error of the micro-XRF analysis is in many cases <10%.

3.5. Analysis of ancient ceramics

The composition of the six most frequently analysed elements in ancient ceramics are presented in Table 3 as % (m/m) ± S.D. oxide for the 12 samples from ancient Abdera (Fig. 9). Characteristic spectra of two samples are presented in Fig. 10. A triangular SiO_2–K_2O–CaO diagram for all samples is presented

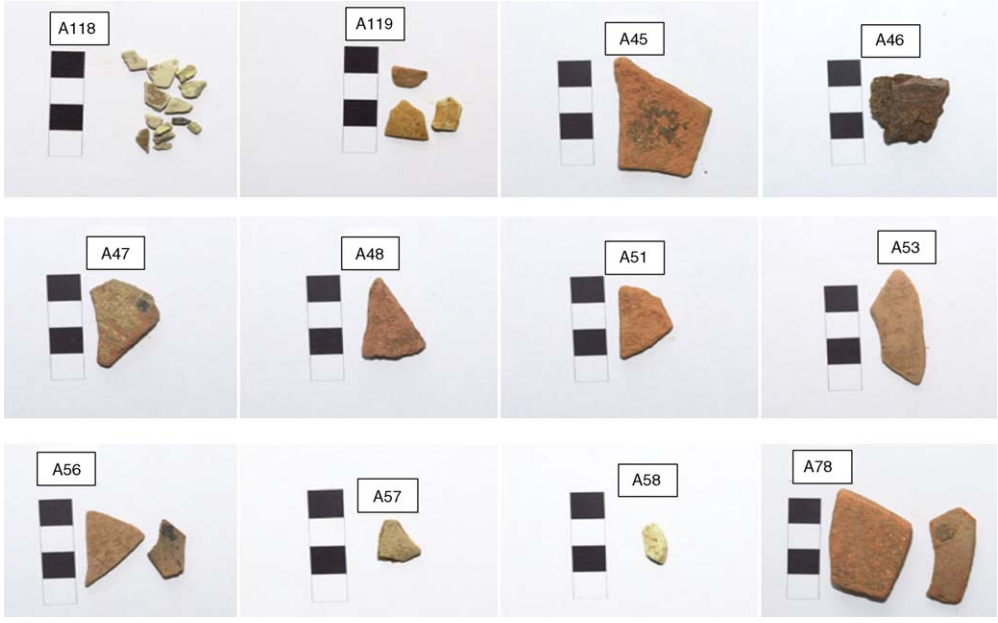

Fig. 9. Photographs of the ancient ceramic sherds.

Table 3
Quantitative analysis of ancient ceramic sherds from ancient Abdera (% (m/m) ± S.D.)

Sample	SiO_2	Fe_2O_3	CaO	MnO	TiO_2	K_2O
A45	48.1 ± 0.7	8.29 ± 0.12	0.61 ± 0.02	0.860 ± 0.011	0.894 ± 0.036	2.17 ± 0.02
A46	50.5 ± 0.6	9.78 ± 0.11	2.18 ± 0.05	1.104 ± 0.013	1.101 ± 0.051	1.88 ± 0.02
A47	46.5 ± 0.7	7.86 ± 0.10	1.21 ± 0.04	0.829 ± 0.011	0.892 ± 0.042	1.72 ± 0.02
A48	51.8 ± 0.7	6.51 ± 0.12	0.68 ± 0.03	0.904 ± 0.011	0.923 ± 0.042	2.23 ± 0.02
A51	40.9 ± 0.6	7.51 ± 0.09	0.48 ± 0.02	0.794 ± 0.012	0.873 ± 0.040	1.73 ± 0.02
A53	49.7 ± 0.7	6.51 ± 0.08	5.39 ± 0.18	0.897 ± 0.011	0.740 ± 0.034	1.03 ± 0.01
A56	58.3 ± 0.7	8.03 ± 0.12	5.46 ± 0.20	1.067 ± 0.014	1.029 ± 0.047	0.91 ± 0.01
A57	57.6 ± 0.8	8.17 ± 0.11	2.57 ± 0.11	1.778 ± 0.021	1.045 ± 0.049	3.06 ± 0.03
A58	34.9 ± 0.6	7.39 ± 0.10	13.39 ± 0.49	1.072 ± 0.014	0.695 ± 0.224	0.62 ± 0.01
A78	42.4 ± 0.6	7.79 ± 0.10	4.43 ± 0.17	0.742 ± 0.011	1.029 ± 0.048	1.41 ± 0.02
A118	36.6 ± 0.4	6.05 ± 0.04	14.88 ± 0.36	0.943 ± 0.007	0.589 ± 0.019	0.39 ± 0.01
A119	36.9 ± 0.4	8.24 ± 0.08	14.18 ± 0.35	1.085 ± 0.010	0.800 ± 0.026	0.70 ± 0.01

in Fig. 11a. The concentrations are normalized in this case (e.g. $C_{Si} = C_{Si}/C_{Si} + C_{Ca} + C_K$). In the case of ancient ceramics, it is most meaningful to use the concentrations of the major and minor elements in order to construct triangular diagrams. Extrapolation can be regarded insignificant, since for some ancient ceramics it is mainly the concentrations of Ca and Si that are outside the range of calibration.

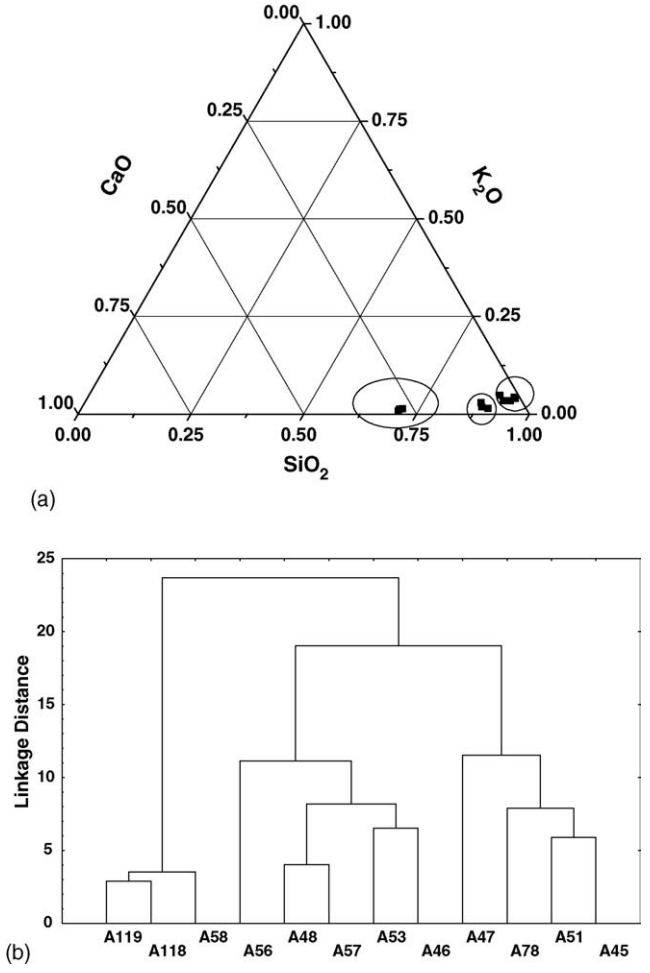

Fig. 11. (a) Triangular diagram showing the grouping of the 12 analysed samples. (b) Complete linkage dendrogram.

According to Fig. 11a, the 12 samples fall into three groups. Data were also statistically treated by a cluster analysis. A hierarchical cluster analysis was performed with complete linkage and evaluation of Euclidean distances (Fig. 11b). The cluster dendrogram with complete linkage Euclidean distances is also presented in Fig. 11b. Samples A119, A118 and A58, which were considered as imported products, group into a single cluster. Moreover, the remaining ceramic samples fall into a cluster with two smaller sub-clusters, as it is also depicted in Fig. 11a.

4. Conclusions

The analytical characteristics of a portable micro-XRF instrument have been determined in this work. The X-ray beam size is 126 μm as recorded by scanning a 50 μm thick Ni wire. The effect of the angle of incidence upon the elemental peak areas was studied for three ancient ceramic samples, each representative of a particular grain size distribution (fine, medium and coarse). As a general observation, the peak areas of all elements are decreased with increasing values of the incidence angle. The peak area reduction ranged from 8 to 14% for a fine texture sample and from 6 to 26% for a medium texture sample, respectively. Therefore, for accurate and reproducible quantitative measurements, it is essential to precisely reproduce the counting geometry. The DL's that were calculated as 3 s values for a ceramic and a glass standard material (SARM 69 and SRM 620, respectively) are in the order of 7–62 mg kg^{-1}, for elements with atomic number 19–30. A quantitative analysis of the standard reference materials SARM 69, SRM 620, NCS DC 73332, AWI-1 and PRI-1 has revealed that the current portable micro-XRF instrument offers the possibility to perform precise, accurate and non-destructive analysis. A quantitative analysis of ceramic sherds from ancient Abdera and a statistical treatment of the respective compositional data, revealed that the current micro-XRF instrument can be successfully applied for the analysis of ancient ceramics and contribute to the interpretation of archaeological issues.

Acknowledgment

The current project was funded by the Greek General Secretariat of Research and Technology and the EU, in terms of the Programme PENED 2001 (Project 01ED240).

References

[1] M. Mantler, M. Schreiner, X-Ray Spectrom. 29 (2000) 3.
[2] M. Milazzo, Nucl. Instrum. Methods Phys. Res. Sec. B 213 (2004) 683.
[3] R.E. Van Grieken, A.A. Markowicz, Handbook of X-Ray Spectrometry, Marcel Dekker, NY, 1993.
[4] A.E. Pillay, C. Punyadeera, L. Jacobson, J. Eriksen, X-Ray Spectrom. 29 (2000) 53.
[5] D.A. Scott, Archaeometry 43 (2001) 475.
[6] O. Williams-Thorpe, P.J. Potts, P.C. Webb, J. Arch. Sci. 26 (1999) 215.
[7] C. Punyadeera, A.E. Pillay, L. Jacobson, G. Whitelaw, X-Ray Spectrom. 26 (1997) 249.
[8] M. Milazzo, C. Cicardi, X-Ray Spectrom. 26 (1997) 211.
[9] K. Janssens, F. Adams, A. Rindby, Microscopic X-Ray Fluorescence Analysis, Wiley, Chichester, 2000.
[10] K. Janssens, B. Vekemans, L. Vincze, F. Adams, A. Rindby, Spectrochim. Acta B 59 (1996) 1661.
[11] S.B. Dabagov, A. Marcelli, G. Cappuccio, E. Burattini, Nucl. Instrum. Methods Phys. Res. Sec. B 187 (2002) 169.
[12] H. Bronk, S. Rohrs, A. Bjeoumikhov, N. Langhoff, J. Schmalz, E.R. Wedell, H.E. Gorny, A. Herold, U. Waldschlager, Fresenius J. Anal. Chem. 371 (2001) 307.
[13] Y. Hosokawa, in: K. Tsuji, J. Injuk, R. Van Grieken (Eds.), X-ray Spectrometry: Recent Technological Advances, John Wiley & Sons, Chichester, 2004.
[14] N. Gao, K. Janssens, in: K. Tsuji, J. Injuk, R. Van Grieken (Eds.), X-Ray Spectrometry: Recent Technological Advances, John Wiley & Sons, Chichester, 2004.
[15] P.A. Pella, M. Lankosz, X-Ray Spectrom. 26 (1997) 327.
[16] F. Adams, A. Adriaens, A. Aerts, I. De Raedt, K. Janssens, O. Schalm, J. Anal. At. Spectrom. 12 (1997) 257.
[17] S. Bichlmeier, K. Janssens, J. Heckel, D. Gibson, P. Hoffmann, H.M. Ortner, X-Ray Spectrom. 30 (2001) 8.
[18] G.J. Havrilla, X-Ray Spectrom. 26 (1997) 364.
[19] P. Moioli, C. Seccaroni, X-Ray Spectrom. 29 (2000) 48.
[20] G. Vittiglio, K. Janssens, B. Vekemans, F. Adams, A. Oost, Spectrochim. Acta B 54 (1999) 1697.
[21] S. Bichlmeier, K. Janssens, J. Heckel, P. Hoffmann, H.M. Ortner, X-Ray Spectrom. 31 (2002) 87.
[22] C. Zarkadas, A.G. Karydas, Spectrochim. Acta B 59 (2004) 1611.
[23] L. Vincze, K. Janssens, F. Adams, K.W. Jones, Spectrochim. Acta B 50 (1995) 1481.
[24] D.N. Papadopoulou, G.A. Zachariadis, A.N. Anthemidis, N.C. Tsirliganis, J. A. Stratis Spectrochim. Acta B 59 (2004) 1877.